Effect of Pore Structure on Char Oxidation Kinetics

Prior studies have demonstrated that char gasification rates vary with conversion, showing a maximum at an intermediate level. In this work experimentally determined char-air reaction rates and corresponding pore structures are compared to assess the applicability of a previously proposed random pore model and to extract pertinent chemical and physical parameters. Results on six different chars are presented and analyzed to obtain structure parameters, intrinsic kinetics, and activation energies. Agreement between two independent evaluations of the structure parameters demonstrates the degree of applicability of the random pore model and supports the view that rate variations with conversion are controlled by pore structural changes, even though overall rates also include contributions of intrinsic reactivity.

J.-L. SU and

D. D. PERLMUTTER

Department of Chemical Engineering
University of Pennsylvania
Philadelphia, PA 19104

SCOPE

Six char samples were generated from two coals by varying pyrolysis heating rate and temperature, and the initial pore structures of the chars were examined by a combination of mercury porosimetry, N_2 adsorption at 77 K, CO_2 adsorption at 195 and 273 K, and pycnometry. For each char, oxidation rates and surface areas were measured in the kinetic control regime at various levels of conversion. By applying a prior random pore model, the intrinsic oxidation kinetics were obtained freed from the structural interference. In order to assess the applicability of this model, values of a pore structure parameter obtained by fitting the kinetic data were compared with values determined from direct measurements on the initial pore structure of the chars.

CONCLUSIONS AND SIGNIFICANCE

Chars with different pore structures can be generated from the same coals by varying pyrolysis conditions: a higher final pyrolysis temperature or a slower heating rate generate chars of more compact structure. The difference in pore structure of chars affects their subsequent oxidation rates. In the kinetic control regime the oxidation rate for each of six chars was observed to change with conversion, showing a local maximum at the same intermediate level, irrespective of reaction temperature.

Normalized reaction rates were compared with normalized surface area changes at different temperatures. The agreement suggested that the rate variations with conversion are controlled by pore structural changes, even though the overall rates were shown to be a combination of contributions of pore structure and intrinsic reactivity. The pore structure parameters obtained from fitting the kinetic data were compared with the values determined by direct measurements on the initial pore structures of the chars. The agreement among these independent evaluations demonstrated the degree of applicability of the random pore model.

INTRODUCTION

A variety of studies on char gasification (Jenkins et al., 1973; Hippo and Walker, 1975; Tomita et al., 1977; Dutta et al., 1977; Dutta and Wen, 1977) have demonstrated that measured reaction rate changes with conversion, showing a maximum rate at an intermediate conversion level. The physical structure of the solid reactant also changes continuously as reaction proceeds, and this evolution of pore structure affects the reaction kinetics by altering the availability of reaction surface area. To account for this effect of the structural changes, a model was proposed by Bhatia and Perlmutter (1980), and independently by Gavalas (1980), that interprets conversion data and the changes of reaction surface area in terms of a combination of chemical and pore size effects. This random pore model expresses reaction rate as

$$\frac{dX}{d\tau} = \frac{S}{S_0} = (1 - X)\sqrt{1 - \psi \ln(1 - X)} \qquad (1)$$

where

$$\psi = \frac{4\pi L_0(1-\epsilon_0)}{S_0^2} = \text{a structure parameter} \quad (2)$$

and

$$\tau = \frac{k_s C_0^n S_0 t}{(1-\epsilon_0)} = \text{a kinetic time parameter} \quad (3)$$

The required information on porosity, surface area, and pore length can be determined from pore volume distribution data obtained before the chemical changes occur by evaluating the integrals

$$\epsilon_0 = \int_0^\infty v(r)dr \quad (4)$$

$$S_0 = 2\int_0^\infty \frac{v(r)}{r}dr \quad (5)$$

and

$$L_0 = \frac{1}{\pi}\int_0^\infty \frac{v(r)}{r^2}dr \quad (6)$$

Alternatively, in the event that surface area and pore length are obtained per unit weight of the solid, the unit conversions

$$L_0 = L_0'\rho_b \quad (7)$$

and

$$S_0 = S_0'\rho_b \quad (8)$$

can be combined with Eq. 2 to give

$$\psi = \frac{4\pi L_0'(1-\epsilon_0)}{\rho_b S_0'^2} \quad (9)$$

Finally, since the ratio $[(1-\epsilon_0)/\rho_b]$ is the reciprocal of the true density, the structural parameter can also be written as

$$\psi = \frac{4\pi L_0'}{\rho_t S_0'^2} \quad (10)$$

By coupling these results with diffusional limitations, this model has been applied to interpret measurements on the reactions of porous lime with SO_2 and CO_2 (Bhatia and Perlmutter, 1981, 1983).

Preliminary tests of this model on char gasification were carried out by Bhatia and Perlmutter (1980) by fitting the experimental data of Hashimoto et al. (1979) and by Gavalas (1980) by fitting the data of Mahajan et al. (1979) and Dutta and Wen (1977). The comparisons are inconclusive, however, since the fitted rate data provide no independent information on the pore structures of the solid reactants. In the work reported here experimentally determined char-air reaction rates and corresponding pore structures are compared for each char tested to assess the applicability of the random pore model and to extract pertinent chemical and physical parameters. The central objective is to separate pore structure analysis from surface reaction kinetics in char gasification.

TABLE 2. CHAR SAMPLES AND THEIR PREPARATION CONDITIONS

Char Sample	Parent Coal	Pyrolysis Heating Rate, K/min	Final Pyrolysis Temp., K
A	PSOC-80	10	873
B	PSOC-4	10	873
C	PSOC-4	10	1,023
D	PSOC-4	10	1,223
E	PSOC-4	5	873
F	PSOC-4	1	873

EXPERIMENT

Sample Preparation

Chars were prepared by pyrolyzing coals under nitrogen. An approximately 1 g sample of coal was placed in a ceramic boat inside a quartz tube within a furnace. The temperature was raised at a controlled heating rate until it reached the preset final pyrolysis temperature. The samples remained in the furnace as they cooled to room temperature under the nitrogen flow.

Two types of coals from the DOE-Penn State Coal Bank were used in these preparations: PSOC-80, a high rank anthracite, and PSOC-4, a lower rank volatile bituminous coal, chosen for their contrasting physical and chemical properties. The proximate and ultimate analyses, as well as pore structure information for thees two coals, are given in Table 1. In all, six different char samples, designated A to F in Table 2, were prepared by varying pyrolysis heating rates and final temperatures. Since the anthracite was relatively more stable during pyrolysis than the bituminous coal, only one char sample was generated from PSOC-80.

Pore Structure Measurement

A Micromeritics model 910 mercury porosimeter was used to study the macropore structure of chars. Pores of radii less than 17 Å were analyzed by absorption techniques using a Quantasorb System (Quantachrome Co.. Nitrogen absorption at 77 K and CO_2 adsorption at 195 K and 273 K were measured, and isotherms were analyzed by the BET equation or the Du-

TABLE 1. CHEMICAL AND PHYSICAL PROPERTIES OF COAL SAMPLES

A. Chemical Compositions (Spackman et al., 1976)

Coal Sample	Rank (Location)	Ultimate Analysis Carbon %	H %	N %	O %	S %	Proximate Analysis Ash %	Volatile Matter %	Water Content %
PSOC-80	Anthracite (Pennsylvania)	78.18	2.25	0.66	4.42	0.55	12.94	5.77	2.51
PSOC-4	HVA bituminous (Kentucky)	82.10	5.67	1.52	1.78	0.86	2.07	37.51	2.48

B. Pore Structure (Gan et al., 1972)

Coal Sample	Pore Volume, cm^3/g >300 Å	12–300 Å	<12 Å	Total
PSOC-80	0.009	0.010	0.057	0.076
PSOC-4	0.017	0.000	0.016	0.033

TABLE 3. SURFACE AREAS OF UNREACTED CHARS DETERMINED BY SEVERAL METHODS

Samples	By Mercury Penetration, m^2/g s >35 Å	s >300 Å	By Gas Adsorption, m^2/g S_{BET} N_2 at 77 K	S_{BET} CO_2 at 195 K	S_m CO_2 at 273 K
A	1.8	0.37	0.87	174	201
B	12.3	1.91	2.42	246	275
C	6.3	1.68	2.45	186	251
D	5.9	1.05	0.39	87	143
E	13.4	4.86	5.05	214	222
F	4.0	0.55	0.51	198	166

binin-Polanyi equation, as appropriate (Brunaur, 1945; Dubinin, 1960). Surface areas evaluated by these several different methods are presented in Table 3. As shown, the nitrogen results are similar to those obtained from mercury intrusion porosimetry for macropores with radii larger than 300 Å, but two orders of magnitude smaller than the results obtained from CO_2 absorption. This finding is consistent with the expectation that nitrogen molecules cannot enter micropores fast enough at low temperatures, as argued by Zwietering and Van Krevelen (1954, 1956) and Walker and Kini (1965).

Further evidence of activated diffusion was found in the slow approach to equilibrium of the nitrogen runs. Since adsorption was incomplete even after 12 h, it was concluded that nitrogen adsorption at 77 K is not adequate for measuring surface on these chars. With only one exception the values of S_m obtained from CO_2 adsorption at 273 K are consistently higher than S_{BET} obtained from CO_2 adsorption at 195 K, suggesting the likelihood of activated diffusion at 195 K. The CO_2 adsorption at 273 K was therefore adopted for all the subsequent surface area measurements. Replicate runs on three specimens taken from the same batch of char typically gave values of S_m within 4% of the mean.

Complete initial pore structures for all char samples were obtained by combining porosimetry with adsorption. The results are presented as Figures 1 and 2 in the form of pore volume distributions with respect to pore radius, showing that three size ranges exist in the char samples: (1) macropores with pore radius larger than 300 Å, (2) mesopores with pore radius between 15 and 300 Å, and (3) micropores with pore radius between 5 and 15 Å. The mesopore region becomes less significant at higher pyrolysis temperatures. For coal type PSOC-4 pyrolyzed to above 873 K, faster heating rates or lower final pyrolysis temperatures produce chars with larger porosity for all sizes of pores, presumably because chars with more open pore structure are produced by the increased gas bubble formation resulting from the breakage of aliphatic chains during the plastic stage of pyrolysis. Higher pyrolysis temperatures are reported to generate a more orderly and compact orientation for aromatic, graphitelike layers, thus reducing the porosity of the chars (Cameron and Stacy, 1958, 1959; Toda, 1973a,b). The anthracite char (sample A) showed a more uniform pore structure with 75% of the pore volume contained in the micropores and with no pores larger than 2000 Å in radius.

The porosities for all char samples listed in Table 4 were calculated from the total pore volume V_T and the true particle density ρ_t by

$$\epsilon = V_T/(V_T + 1/\rho_t) \tag{11}$$

For this purpose a specially made sample cell volume calibrated at the factory allowed the determination of true powder density by measuring the volume of a weighed sample, excluding pore volume. A summary of the pore structure results for all six char samples is presented in Table 4. It may be noted that macropores generally contribute a substantial portion of the total pore volume but are insignificant in their contribution to the total surface area (less than 5%) and almost completely negligible in the calculation of pore length. The pore length, in fact, can be calculated solely from the micropore volume distribution. It is also apparent from Table 4 that the ψ values of these chars range only within 7 to 10, although their detailed pore structures are quite different. This is a consequence of the fact that for a char with relatively open pore structure, the larger surface area S_0' is usually compensated for by a larger L_0' and a smaller true density ρ_t.

Reaction Rates

The reactivity in air of each char sample was measured in a Dupont model 951 Thermogravimetric Analyzer (TGA). The reaction chamber was purged with nitrogen for 30 min before the temperature was rapidly raised to the desired reaction temperature. The reaction was initiated by introducing high purity, dried air at a controlled flow of 100 mL/min. The air temperature, the sample weight, and the time derivative of weight loss were continuously recorded. For reactions at different gas concentrations, the air was diluted with nitrogen to obtain the desired oxygen partial pressures. The particle temperature rise for these reactions was computed by Su (1983) not to exceed 3.1 K. To prepare partially reacted samples for structural analysis, the reaction was terminated at the desired conversion levels by purging nitrogen through the reaction chamber. TGA results showed that weight loss can be stopped within 1 min. Further experimental details are given by Su (1983).

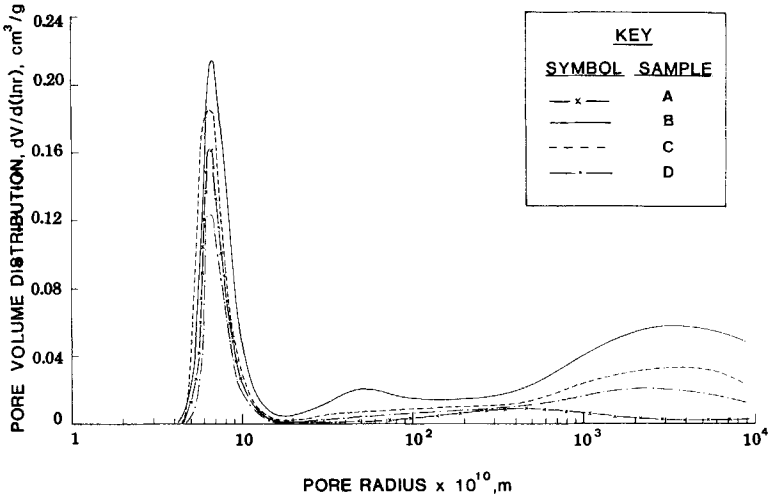

Figure 1. Pore size distribution for char samples A, B, C, and D.

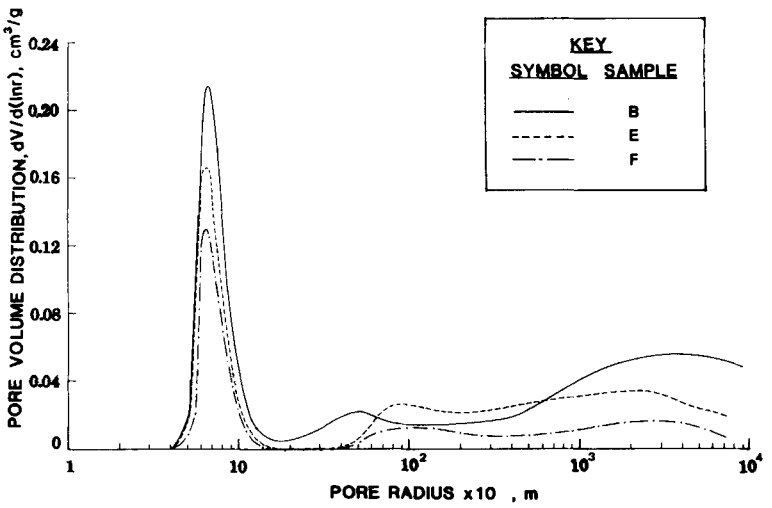

Figure 2. Pore size distribution for char samples B, E, and F.

RESULTS AND DISCUSSION

Rate Controlling Regime

To establish the experimental conditions for which the reaction is chemical kinetics controlled, the char-air reaction rates of the most reactive char sample (sample B) were first measured over the temperature range of 653 to 803 K for various particle sizes. It was found that reducing particle size in the range of 250 to less than 100 μm did not produce an appreciable difference in reaction rate until temperature exceeded 728 K. Apparent activation energy was also found to decrease noticeably for reaction temperature greater than 728 K, indicating that interparticle diffusion became significant at such temperatures. The reactions were therefore in the regime of chemical kinetic control at reaction temperatures less than 728 K for sample B as well as for the other less reactive char samples with particle size of 250 μm or smaller. Such reaction conditions also have been shown by other workers to be in the chemical kinetic control regime for char-air reactions (Smith and Tyler, 1974; Dutta and Wen, 1977).

Rate vs. Conversion

The changes of overall char-air reaction rate with conversion were measured in the chemical kinetic control regime for char samples A to F. The results are presented in Figure 3 to 8, expressed in terms of percentage conversion of the reactive carbonaceous materials in the unreacted chars, excluding the nonreactive ash content. Three replicate runs for each of samples B, C, and D at

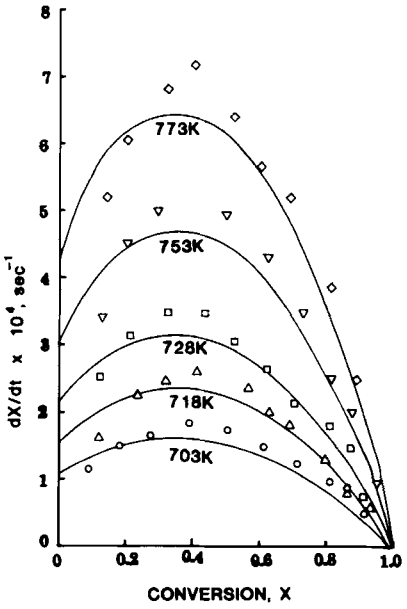

Figure 3. Char-air reaction rates for sample A at different temperatures. The curves are fitted by random pore model.

TABLE 4. PORE STRUCTURE PARAMETERS FOR UNREACTED CHAR SAMPLES

Sample	True Density, g/cm³	Macropores Volume, cm³/g	Macropores Surface, m²/g	Micropores Volume, cm³/g	Micropores Surface, m²/g	Total Pores Volume, cm³/g	Total Pores Surface, m²/g	Pore Length, m/g	Porosity	Structure Parameter, ψ
A	1.41	0.025	1.8	0.074	201	0.099	203	4.69×10^{10}	0.12	10.1
B	1.42	0.187	12.3	0.098	275	0.285	287	6.40×10^{10}	0.29	6.88
C	1.61	0.113	6.3	0.085	251	0.198	257	6.13×10^{10}	0.24	7.24
D	1.82	0.080	5.9	0.054	143	0.134	149	3.16×10^{10}	0.30	9.83
E	1.54	0.152	13.4	0.076	222	0.228	235	5.37×10^{10}	0.26	7.93
F	1.63	0.051	4.0	0.059	166	0.110	170	3.85×10^{10}	0.15	9.68

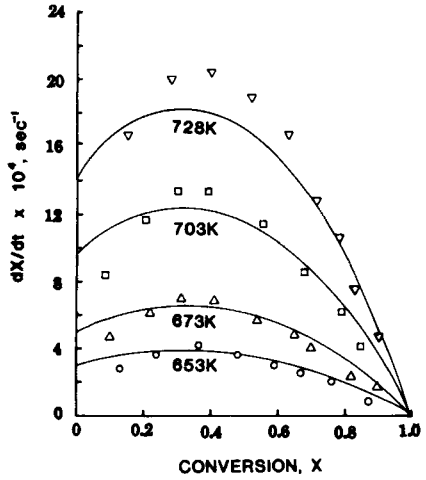

Figure 4. Char-air reaction rates for sample B at different temperatures. The curves are fitted by random pore model.

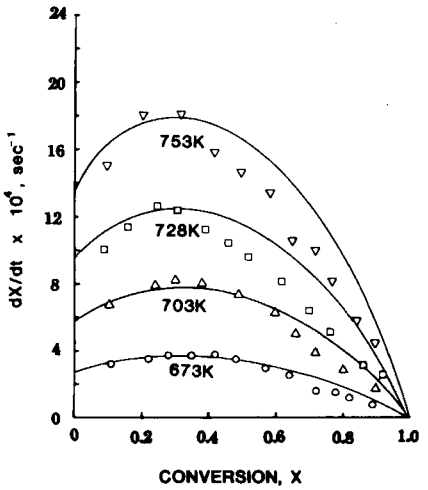

Figure 5. Chair-air reaction rates for sample C at different temperatures. The curves are fitted by random pore model.

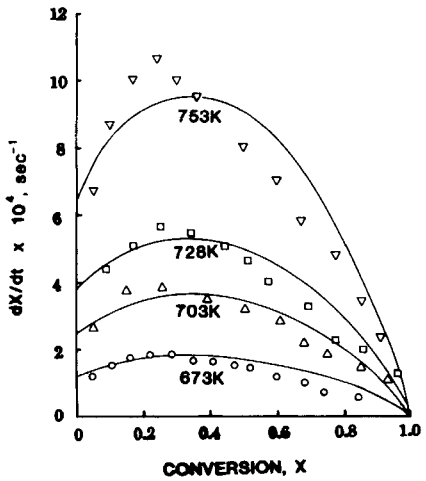

Figure 6. Char-air reaction rates for sample D at different temperatures. The curves are fitted by random pore model.

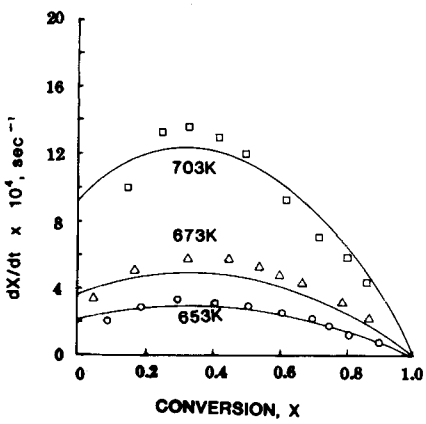

Figure 7. Char-air reaction rates for sample E at different temperatures. The curves are fitted by random pore model.

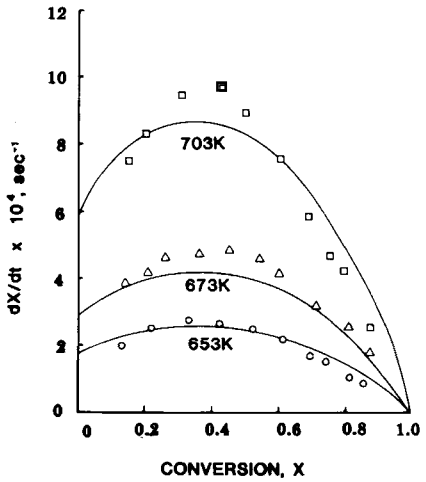

Figure 8. Char-air reaction rates for sample F at different temperatures. The curves are fitted by random pore model.

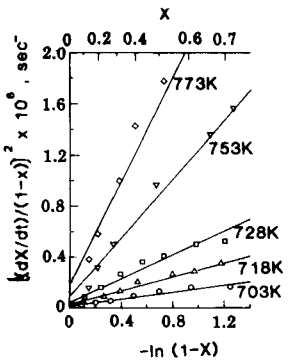

Figure 9. Correlation of rate data of sample A with random pore model.

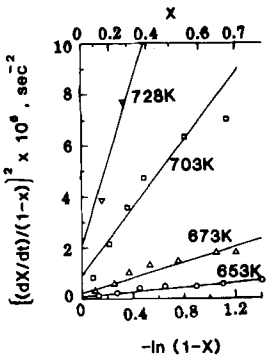

Figure 10. Correlation of rate data of sample B with random pore model.

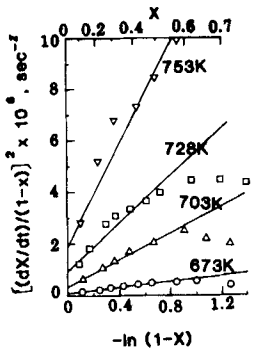

Figure 11. Correlation of rate data of sample C with random pore model.

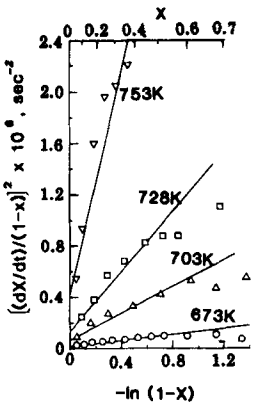

Figure 12. Correlation of rate data of sample D with random pore model.

673 K showed that the variations of the measured rates are within 10%. Comparison of Figures 4 to 8 for the bituminous chars shows that increasing pyrolysis heating rate from 1 to 10 K/min increases the subsequent overall oxidation rate by about 30%, while decreasing ultimate pyrolysis temperature from 1,223 to 873 K causes an overall rate increase of almost 400% for all reaction temperatures tested under 728 K.

The most straightforward test of the random pore model may be formulated in terms of the pore structure parameter ψ. This parameter can be obtained by either of two independent means.

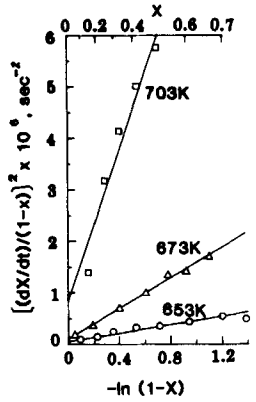

Figure 13. Correlation of rate data of sample E with random pore model.

First, ψ can be obtained from direct measurements on the initial pore structure of a char as shown in Table 4. Second, the same parameter can also be extracted from an appropriate fit of the kinetic reaction rate data to the random pore model. For this purpose the rate data are shown again in Figures 9 to 14, but on coordinates chosen to give linear dependence according to the rearranged Eq. 1 in the form

$$\left[\frac{dX/dt}{1-X}\right]^2 = \left[\frac{k_s C_o^n S_o}{1-\epsilon_o}\right]^2 - \psi\left[\frac{k_s C_o^n S_o}{1-\epsilon_o}\right]^2 \ln(1-X) \qquad (12)$$

One can obtain the intrinsic reaction rate $k_s C_o^n$ from the intercept at $X = 0$ and the pore structure parameter ψ from the ratio of slope to intercept.

Linear regressions in Figures 9 to 14 give values of slopes with ±5 to ±25% variations within 90% confidence levels. The variations of intercepts at the same confidence levels are significantly larger, in the range of ±19 to ±60%. As a consequence, the values of ψ obtained as the ratio of slopes to intercepts carry variations in the range of ±20 to ±66%. The pore structure parameters extracted from these fits to the kinetic data are shown in Table 5 and compared to those obtained from the direct pore structure measurements. Since the pore structure parameter is characteristic of only the solid physical properties, the values obtained from kinetic data should be the same regardless of the reaction temperatures. Although the results in Table 5 show some variation, their averaged values are in agreement with those obtained from direct pore structure measurement within the 90% confidence level.

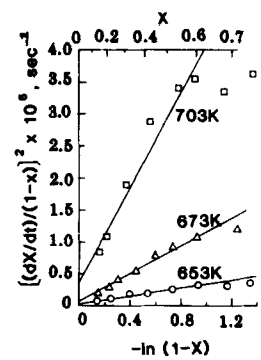

Figure 14. Correlation of rate data of sample F with random pore model.

TABLE 5. COMPARATIVE VALUES OF PORE STRUCTURE PARAMETER OBTAINED BY TWO INDEPENDENT TECHNIQUES

Sample	Pore Structure Parameter ψ By Fit to Kinetic Data Reaction Temperature, K 653	673	703	718	728	753	773	Average	By Direct Physical Measurement
A	—	—	12.04 ± 7.22	11.00 ± 3.96	10.22 ± 4.91	12.05 ± 5.78	10.97 ± 7.2	11.26 ± 2.66	10.14
B	5.11 ± 3.07	6.00 ± 3.36	7.17 ± 2.87	—	8.13 ± 2.68	—	—	6.60 ± 1.50	6.88
C	—	7.67 ± 3.53	7.59 ± 1.52	—	5.17 ± 1.50	5.41 ± 31.4	—	6.46 ± 1.30	7.24
D	—	8.11 ± 2.84	8.43 ± 3.03	—	9.04 ± 2.71	10.32 ± 5.78	—	8.98 ± 1.90	9.83
E	8.62 ± 5.40	11.60 ± 3.94	9.03 ± 3.79	—	—	—	—	9.75 ± 2.56	7.93
F	10.17 ± 4.27	13.50 ± 5.67	10.71 ± 5.25	—	—	—	—	11.46 ± 2.94	9.68

TABLE 6. INTRINSIC CHAR-AIR REACTION RATES AND ACTIVATION ENERGIES

Sample	Intrinsic Reaction Rate $(k_s C_o^n \rho t) \times 10^6$, g of Char/s · m² Surface Reaction Temperatures, °C 380	400	430	445	455	480	500	Activation Energy, kcal/mol
A	—	—	0.53 ± 0.32	0.78 ± 0.27	1.05 ± 0.42	1.52 ± 0.61	21.3 ± 1.28	23.5 ± 1.2
B	0.94 ± 0.56	1.74 ± 0.84	3.34 ± 1.14	—	4.90 ± 1.52	—	—	2.15 ± 3.0
C	—	1.07 ± 0.47	2.27 ± 0.43	—	3.70 ± 0.96	5.30 ± 2.65	—	22.5 ± 2.2
D	—	0.82 ± 0.27	1.66 ± 0.58	—	2.41 ± 0.70	4.33 ± 2.25	—	22.5 ± 2.1
E	0.92 ± 0.552	1.51 ± 0.51	3.85 ± 1.50	—	—	—	—	26.5 ± 4.5
F	1.02 ± 0.41	1.67 ± 0.70	3.49 ± 1.39	—	—	—	—	23.7 ± 4.3
Lewis and Simon correlation (1979)	0.14	0.33	1.10	1.93	2.78	6.61	12.69	

The agreement in the independent evaluations of ψ demonstrates the degree of applicability of the random pore model, but several likely sources of deviation should be noted. First, it is possible that particles may disintegrate at high conversions; if so, the model becomes inapplicable. Furthermore, relatively small deviations in dX/dt at high conversion level (e.g., $X = 0.8$) can be magnified to a deviation in $[(dX/dt/(1 - X)]^2$ more than 20-fold larger by the square and the denominator factor $(1 - X)$. Finally, the larger than expected rates in the conversion range of the rate maximum may be due to the temperature rise of the reacting particle. In fact, using the estimated maximum temperature rise of 3.1 K and the activation energy of 23 kcal/mol (see Table 6), the rate increase caused by temperature rise is calculated to be about 7% to 728 K. This value is close to the deviations shown in Figures 9 to 14 in the 20 to 50% conversion ranges. With these limitations in mind, only the rate data up to 60% conversion were used to extract the parameters of interest.

Intrinsic Chemical Rates

The intrinsic reaction rates $k_s C_o^n$ of the char samples were obtained from the intercepts of Figures 9 to 14 and put on a weight basis for listing in Table 6. Samples B, E, and F have essentially the same intrinsic rates, although their overall rates are about 30% different, indicating that the differences in the overall reaction raes are attributable to the differences in initial and developed physical structure rather than surface chemistry. This conclusion may be supported by the pyrolysis results: The weight loss at a pyrolysis temperature of 873 K was unaffected by heating rate, suggesting that samples B, E, and F probably have similar chemical composition. Similarly, although decreasing pyrolysis temperatures from 1,223 to 873 K causes almost fourfold increases of overall oxidation rate, the intrinsic rate of sample B is only about twice as large as that of sample D. These results indicate that the contributions of physical effects to overall reaction rates are significant, and the overall reaction rates one measures should not be used to compare char reactivities directly. Also shown in Table 6 for comparison are intrinsic reaction rates with air calculated from the correlation of Lewis and Simons (1979) in the form

$$\text{rate} = \frac{k_2 k_1 P_{O_2}}{k_2 + k_1' + k_1 P_{O_2}} \times 10^4 \ (g\ of\ carbon/m^2 \cdot s) \quad (13)$$

where

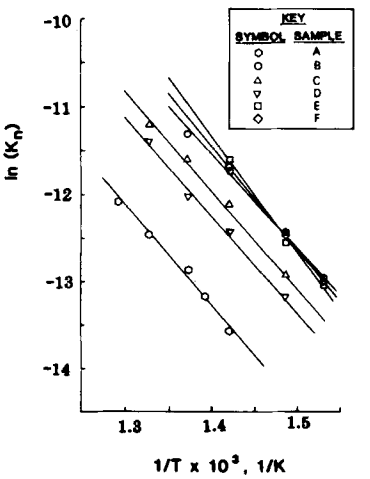

Figure 15. Rate constants for char-air reactions of samples A to F.

TABLE 7. TOTAL SURFACE AREAS OF CHARS AT DIFFERENT LEVELS OF CONVERSION*

Sample	Temp., K	Conversions, % 0	15	30	45	60	75
A	703	201(201)	280(245)	368(275)	394(245)	395(196)	351(130)
	728	201(201)	302(264)	374(380)	442(275)	479(283)	451(167)
B	653	275(275)	336(290)	392(385)	409(241)	425(193)	376(120)
	673	275(275)	354(306)	366(266)	437(258)	439(199)	398(126)
	703	275(275)	364(314)	389(282)	425(251)	441(200)	445(141)
C	673	251(251)	343(297)	396(290)	400(240)	404(188)	380(126)
	703	251(251)	337(292)	407(298)	449(269)	438(204)	412(137)
	728	251(251)	353(306)	417(306)	495(297)	478(223)	415(138)
D	673	143(143)	214(187)	284(212)	302(186)	311(152)	328(119)
	703	143(143)	206(180)	266(198)	314(194)	290(142)	287(104)
	728	143(143)	206(180)	258(192)	303(187)	316(155)	268(97)
E	653	222(222)	317(274)	392(285)	440(260)	447(203)	406(129)
	673	222(222)	306(264)	389(283)	383(226)	403(183)	364(116)
	703	222(222)	325(281)	395(287)	428(253)	445(202)	460(146)
F	653	166(166)	279(241)	348(253)	400(236)	396(180)	403(128)
	673	166(166)	301(260)	362(263)	385(227)	378(172)	385(122)
	703	166(166)	271(234)	344(250)	276(222)	423(192)	485(154)

* Results are expressed in m^2/g of partially reacted sample as well as in m^2/g of unreacted sample (in parentheses).

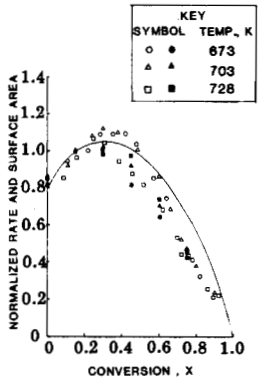

Figure 16. Effect of conversion on reaction rate (open points) and pore surface area (filled points) at different reaction temperatures for sample C. Both are normalized with respect to the values at 15% conversion. The line is a fit of the random pore model.

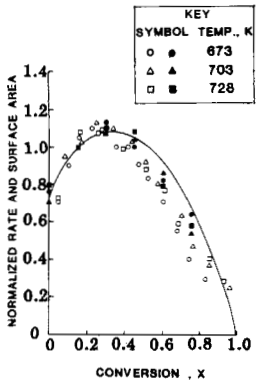

Figure 17. Effect of conversion on reaction rate (open points) and pore surface area (filled points) at different reaction temperatures for sample D. Both are normalized with respect to the values at 15% conversion. The line is a fit of the random pore model.

$$k_1 = 900 \exp(-19{,}000/T)$$
$$k_2 = 90 \exp(-19{,}000/T)$$
$$k_1' = 200\, k_1 k_2 \exp(-3{,}500/T)$$

The results agree within an order of magnitude with those obtained in this study by the random pore model.

A set of experiments was conducted to determine the order of the reactions. Both samples A and B were reacted at 703 K with oxygen at partial pressures ranging from 5×10^3 to 2×10^4 Pa. The intrinsic rates were found to vary linearly with oxygen partial pressure, a first-order reaction in this pressure range. Figure 15 shows the rate constants on Arrhenius coordinates. The activation energies of these samples were found to be similar, all in the range of 21 to 27 kcal/mole (Table 6).

Changes of Surface Area with Reaction

The development of the char surface areas during reaction was determined for each of the chars as they reacted with air at various temperatures to five different levels of conversion (15, 30, 45, 60 and 75%). Results are reported in Table 7 in terms of each of the two bases used: one expressed per unit weight of unreacted solid, the other on a partially-reacted weight basis. The two are related by

$$S_0' = S'[(1 - f)(1 - X) + f] \qquad (14)$$

It may be noted that the surface areas developed were generally unaffected by the reaction temperatures used, further evidence that these reactions were in the regime of chemical kinetic control. When normalized with respect to values at 15% conversion, both surface area conversion and rate conversion dependencies are

TABLE 8. COMPARISONS OF N_2 SURFACE AREA AND CO_2 SURFACE AREA FOR SAMPLE B PARTIALLY REACTED AT 673 K

Conversion, %	CO_2 Surface Area, m^2/g	N_2 Surface Area, m^2/g
0	275	2.4
15	354	195
30	366	267
45	437	340
60	439	351
75	398	342

found to be virtually a single relationship independent of temperature, with both a surface area maximum and rate maximum at an intermediate level of conversion. Typical results are shown in Figures 16 and 17 for samples C and D, indicating that the rate variations are controlled by the physical structural changes during reaction. If the directly measured initial pore structure parameter is used with Eq. 1, the predictions are found to agree with experimental data within approximately ±25%, as shown in Figures 16 and 17.

It was noted above that N_2 adsorption at 77 K was not suitable for surface area determinations of the unreacted chars because of activated diffusion. As chars partially react, however, enlargement of pore sizes could significantly reduce these limitations. Patel et al. (1972) and Walker (1980) have shown that partially gasifying anthracite char can result in changing the diffusion mode from activated diffusion to Knudsen diffusion, with increases of orders of magnitude in the effective diffusivity of methane. The N_2 adsorption at 77 K was thus also used in this study to meausre surface areas of the partially reacted sample B to study the effect of conversion on the activated diffusion resistance. The results are shown in Table 8. In agreement with the prior studies, the nitrogen surface areas increased drastically from 2.4 to 195 m^2/g after only 15% conversion. The greater the conversion, the closer the values found between N_2 and CO_2 surface areas, indicating a steady decrease of activated diffusion resistance resulted from the pore size enlargement. The CO_2 surface areas were still considerably larger, however, than the N_2 surface areas in the low conversion range and probably better represent the real surface areas available for reaction.

ACKNOWLEDGMENT

This research was funded by the U.S. Department of Energy Fossil Research Program under Contract No. EX 76-S-01-2450.

NOTATION

C_0 = ambient concentration of gas reactant, mol/m^3
f = weight fraction ash in sample, dimensionless
k_1, k_2, k_1' = rate constants defined by Eq. 13
k_s = intrinsic reaction rate constant defined by Eq. 3
L_0 = total pore length per unit volume of unreacted particle, m/m^3
L_0' = total pore length per unit weight of unreacted particle, m/g
n = order of reaction, dimensionless
P_{O_2} = partial pressure of oxygen in reaction system, atm
S = total surface area per unit volume of reacting particle, m^2/m^3
S_0 = S at $t = 0$
S' = total surface area per unit weight of reacting particle, m^2/g
S_0' = S' at $t = 0$
S_{BET} = surface area obtained by BET equation, m^2/g
S_m = micropore surface area obtained by Dubinin-Polanyi equation, m^2/g
T = temperature of the reacting particle, K
t = reaction time, s
V_T = total pore volume distribution function per unit volume of particle, dimensionless
X = conversion, dimensionless

Greek Letters

ϵ_o = initial porosity, dimensionless
ρ_b = bulk density of solid particles, g/cm^3
ρ_t = true density of solid particles, excluding pore volume, g/cm^3
τ = $k_s C_o t S_o/(1 - \epsilon_o)$, dimensionless time
ψ = $4\pi L_o(1 - \epsilon_o/S_o^2$, a pore structure parameter

LITERATURE CITED

Bhatia, S. K., and D. D. Perlmutter, "A Random Pore Model for Fluid-Solid Reactions. I. Isothermal, Kinetic Control," *AIChE J.*, **26**, 379 (1980).

———, "The Effect of Pore Structure on Fluid-Solid Reactions: Application to the SO_2-Lime Reaction," *AIChE J.*, **27**, 226 (1981).

———, "Effect of the Product Layer on the Kinetics of CO_2-Lime Reaction," *AIChE J.*, **29**, 79 (1983).

Brunaur, S., *The Adsorption of Gases and Vapors*, p. 75, Oxford University Press, London (1945).

Cameron, A., and W. O. Stacy, "Changes in the Pure Structure of Coke During Carbonization and Gasification," *Austr. J. Appl. Sci.*, **9**, 283 (1958).

———, "The Pore Structure of Chars and Cokes," *Austr. J. Applied Sci.*, **10**, 449 (1959).

Dubinin, M. M., "The Potential Theory of Adsorption of Gases and Vapors for Adsorbents with Energetically Nonuniform Surfaces," *Chem. Rev.*, **60**, 235 (1960).

Dutta, S., C. Y. Wen, and R. J. Belt, "Reactivity of Coal and Char. 1. In Carbon Dioxide Atmospheres," *Ind. Eng. Chem. Proc. Des. Dev.*, **16**, no. 1, 20 (1977).

Dutta, S., and C. Y. Wen, "Reactivity of Coals and Char. 2. In Oxygen-Nitrogen Atmosphere," *Ind. Eng. Chem. Proc. Des. Dev.*, **16**, no. 1, 31 (1977).

Gan, H., S. P. Nandi, and P. L. Walker, Jr., "Nature of the Porosity in American Coals," *Fuel*, **51**, 272 (1972).

Gavalas, G. R., "A Random Capillary Model with Application to Char Gasification of Chemically Controlled Rates," *AIChE J.*, **26**, 577 (1980).

Hashimoto, D., et al., "Change in Pore Structure ofr Carboneaceous Materials During Activation and Adsorption Performance of Activated Carbon," *Ind. Eng. Chem. Proc. Des. Dev.*, **18**, 73 (1979).

Hippo, E., and P. L. Walker, Jr., "Reactivity of Heat-Treated Coals in Carbon Dioxide at 900°C," *Fuel*, **54**, 245 (1975).

Jenkins, R. G., S. P. Nandi, and P. L. Walker, Jr., "Reactivity of Heat-Treated Coals in Air at 500°C," *Fuel*, **52**, 288 (1973).

Lewis, P. F., and G. A. Simons, "Char Gasification. II. Oxidation Results," *Combust. Sci. Technol.*, **20**, 117 (1979).

Mahajan, O. P., R. Yarzab, and P. L. Walker, Jr., "Unification of Coal-Char Gasification Reaction Mechanisms," *Fuel*, **57**, 643 (1978).

Patel, R. L., S. P. Nandi, and P. L. Walker, Jr., "Molecular Sieve Characteristics of Slightly Anthracite," *Fuel*, **51**, 47 (1972).

Smith, I. W., and R. J. Tyler, "The Reactivity of a Porous Brown Coal Char to Oxygen Between 630 and 1812°K," *Combust. Sci. Technol.*, **9**, 87 (1974).

Spackman, W., et al., "Evaluation and Development of Special Purpose Coals," Fossil Energy, Coal Research Sect., Pennsylvania State Univ., September (1976).

Su, J.-L., "Pore Structure and Catalytic Effects on Char Gasification Kinetics," Ph.D. Thesis, p. 403, Univ. of Pennsylvania (1983).

Toda, T., "A Study by Density Measurement of Changes in Pore Structure of Coals with Heat Treatment. 2. Micropore Structure," **Fuel**, *52*, 36 (1973a).

———, "A Study by Density Measurement of Changes in Pore Structures of Coals with Heat Treatment. 2. Micropore Structure," *Fuel*, **52**, 99 (1973b).

Tomita, A., O. P. Mahajan, and P. L. Walker, Jr., "Reactivity of Heat-Treated Coals in Hydrogen," *Fuel*, **56**, 137 (1977).

Walker, P. L., Jr., and K. A. Kini, "Measurement of the Ultrafine Surface Area of Coals," *Fuel*, **59**, 809 (1980).

Zwietering, P., and D. W. Van Krevelen, "Chemical Structure and Properties of Coal. IV. Pore Structure," *Fuel*, **33**, 331 (1954).

Zwietering, P., J. Overeem, and D. Van Krevelen, "Chemical Structure and Properties of Coal. XIII. Activated Diffusion of Gases in Coal," *Fuel*, **35**, 66 (1956).

Manuscript received Mar. 7, 1984; revision received Sept. 10, 1984, and accepted Sept. 11.